LOW-TEMPERATURE MAGNETISM

Distorted diamond Ising-Hubbard chain

B. M. Lisnii[a)]

Institute of Condensed System Physics, National Academy of Sciences of Ukraine, ul. Sventsitskogo 1, Lviv 79011, Ukraine

(Submitted May 26, 2010; revised August 16, 2010)
Fiz. Nizk. Temp. **37**, 380–391 (April 2011)

The ground state and thermodynamics of distorted Ising-Hubbard chains are studied with on-site Coulomb repulsion taken into account. A decoration-iteration transformation method is used to obtain exact results for the free energy, entropy, specific heat, magnetization of the Ising and Hubbard subsystems, and magnetic susceptibility. The effect of Coulomb repulsion on the ground state, field and temperature dependences of the magnetization, magnetic susceptibility, and specific heat is studied for the case of a geometrically frustrated system. Strong repulsion leads to formation of an additional high-temperature peak in the specific heat. Independently of any repulsion, the temperature dependence of the specific heat can have two low-temperature peaks. © *2011 American Institute of Physics*. [doi: 10.1063/1.3592221]

I. INTRODUCTION

One-dimensional models with a regular variation in the interaction between spins and/or in the magnitude of the spins are of interest in statistical mechanics because they can be solved exactly and used to explain the physical properties of complicated real systems. Many such exactly soluble one-dimensional models with a certain type of structure corresponding to a decorated primitive cell of a spin-1/2 Ising chain of a group of spins in interstitial positions, are currently known. Decorated spins can be coupled to one another by various interactions, but they are coupled to vertex (Ising) spins only by an Ising interaction. Decoration-iteration transformations are used to solve these models exactly.[1,2] Examples of models of this type also include Ising chains, e.g., spin (1/2, $S > 1/2$),[3] ferromagnetic-ferromagnetic-antiferromagnetic,[4] and diamond,[5] as well as Ising-Heisenberg chains, where a Heisenberg interaction acts between decorated spins, e.g., simple,[6,7] diamond,[8,9] sawtooth,[10] tetrahedral,[11] and with triangular Heisenberg plaquettes.[12] These models make it possible to study interesting features of various physical characteristics and effects: the magnetization plateau at intermediate magnetizations,[4–10,12] additional low-temperature peaks in the specific heat,[3,5–9,12] geometric frustration,[5,8–12] and the interaction between geometric frustration and quantum fluctuations.[8–12] Interest in these features and effects is heightened by the fact that they are observed in real systems.[8,13,14]

Recently a model has been proposed[15] that consists of a spin-1/2 Ising chain decorated with mobile electrons. This is a distorted diamond Ising-Hubbard chain when on-site (concentric) Coulomb repulsion of the electrons is neglected. In this chain, two mobile electrons make quantum jumps between two interstitial positions located in opposite vertices of a diamond. The lattice point spins and the electron spins are coupled along the sides of a diamond by Ising interactions. Quantum jumps of the electrons control the antiferromagnetic correlation between their spins.[15] Thus, with an antiferromagnetic Ising interaction, this chain represents a geometrically frustrated spin system, analogous to an Ising-Heisenberg diamond chain.[8,9] The Ising-Hubbard chain can be solved exactly by the decoration-iteration transformation method.[1,2] Note that if this were a distorted diamond Hubbard chain, an exact solution could be obtained by a much more complicated procedure only for certain conditions on the model parameters and at very low temperatures.[16] The properties of the ground state, magnetization processes, and the temperature dependences of the magnetization, magnetic susceptibility, and specific heat,[15] as well as the magnetocaloric effect[17] have been studied for distorted diamond Ising-Hubbard chains neglecting on-site Coulomb repulsion. In particular, it has been shown that during magnetization at zero temperature, the magnetization can have an intermediate plateau at a height of 1/3 of the saturation magnetization and that the temperature dependence of the specific heat has a principal and a low-temperature secondary maxima.[15]

This paper is a study of the properties of a distorted diamond Ising-Hubbard chain[15] with the on-site Coulomb repulsion of electrons taken into account. The decoration-iteration transformation method is used to calculate the thermodynamic characteristics exactly. The effect of repulsion on the ground state, magnetization processes, temperature dependences of the system magnetization, magnetization of the Ising and electronic subsystems, and the magnetic susceptibility and specific heat are studied for the case of an antiferromagnetic Ising interaction when the system is geometrically frustrated.

II. MODEL HAMILTONIAN: EXACT CALCULATION OF THERMODYNAMIC CHARACTERISTICS

Let us consider a distorted diamond Ising-Hubbard chain in a magnetic field.[15] The primitive cell of the chain (Fig. 1) is defined by the nodes k and k+1, which are occupied by Ising spins. It contains two interstitial positions (k,1) and (k,2) between which quantum jumps of two mobile electrons take place. A Coulomb repulsion acts between two electrons in a single position. The hamiltonian $\mathcal{H}$ of a chain consisting of N primitive cells is given by the sum of the cell hamiltonians $\mathcal{H}_k$:

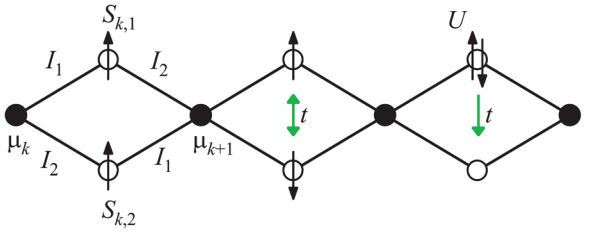

FIG. 1. Illustrating a fragment of a distorted diamond Ising-Hubbard chain. The node spins μ_k, μ_{k+1} and the z-components $S_{k,1}, S_{k,2}$ of the total spins created by two mobile electrons at interstitial positions.

$$\mathcal{H} = \sum_{k=1}^{N} \mathcal{H}_k,$$

$$\mathcal{H}_k = \sum_{\sigma\in\{\uparrow,\downarrow\}} t(c^{\dagger}_{k,1;\sigma}c_{k,2;\sigma} + c^{\dagger}_{k,2;\sigma}c_{k,1;\sigma}) + \sum_{i=1}^{2} U n_{k,i;\uparrow}n_{k,i;\downarrow} + \mu_k(I_1 S_{k,1} + I_2 S_{k,2}) + \mu_{k+1}(I_2 S_{k,1} + I_1 S_{k,2}) - \frac{1}{2}h_i(\mu_k + \mu_{k+1}) - h_e(S_{k,1} + S_{k,2}), \quad (1)$$

where $c^{\dagger}_{k,i;\sigma}$ and $c_{k,i;\sigma}$ are the creation and annihilation operators for an electron with spin $\sigma \in \{\uparrow,\downarrow\}$ at interstitial position (k,i), i = 1,2; $n_{k,i;\sigma} = c^{\dagger}_{k,i;\sigma}c_{k,i;\sigma}$ is the operator for the number of electrons with spin σ at position (k,i); and $S_{k,i} = (n_{k,i;\uparrow} - n_{k,i;\downarrow})/2$ is the z-component of the operator for the total spin of the electrons at position (k,i). The parameters t and U denote the jump integral and the on-site Coulomb repulsion of the electrons. The spin variable μ_k denotes the z-component of the spin-1/2 operator and describes the state of the Ising spin at site k. The parameters I_1 and I_2 describe the Ising interactions along the sides of the diamond between node and interstitial spins of the primitive cell, as shown schematically in Fig. 1. The parameters h_i and h_e describe the effect of the magnetic field on the Ising and electron spins, respectively.

We now find the partition function of this system, $\mathcal{Z} = \mathrm{Tr}\exp(-\beta\mathcal{H})$, where $\beta = 1/k_BT$, k_B is the Boltzmann constant, and T is the absolute temperature. The hamiltonians $\mathcal{H}_k$ commute with each other, so $\mathcal{Z}$ can be partially factored:

$$\mathcal{Z} = \mathrm{Tr}_{\{\mu\}} \prod_{k=1}^{N} \mathrm{Tr}_{\{k,1;k,2\}} \exp(-\beta\mathcal{H}_k), \quad (2)$$

where $\mathrm{Tr}_{\{\mu\}}$ is the trace with respect to the Ising spins and $\mathrm{Tr}_{\{k,1;k,2\}}$ is the trace with respect to the states of the two electrons in cell k.

We now calculate the trace of the operator $\exp(-\beta\mathcal{H}_k)$ with respect to the electron states:

$$\mathcal{Z}_k(\mu_k,\mu_{k+1}) = \mathrm{Tr}_{\{k,1;k,2\}} \exp(-\beta\mathcal{H}_k).$$

To do this, we transform to a matrix representation of the operators $c_{k,i;\sigma}$ and $c_{k,i;\sigma}$ in a basis constructed from the states of the two electrons in the primitive cell:

$$|\uparrow,\uparrow\rangle = c^{\dagger}_{k,1;\uparrow}c^{\dagger}_{k,2;\uparrow}|0\rangle, \quad |\downarrow,\downarrow\rangle = c^{\dagger}_{k,1;\downarrow}c^{\dagger}_{k,2;\downarrow}|0\rangle,$$
$$|\uparrow,\downarrow\rangle = c^{\dagger}_{k,1;\uparrow}c^{\dagger}_{k,2;\downarrow}|0\rangle,$$

$$|\downarrow,\uparrow\rangle = c^{\dagger}_{k,1;\downarrow}c^{\dagger}_{k,2;\uparrow}|0\rangle, \quad |\uparrow\downarrow,0\rangle = c^{\dagger}_{k,1;\uparrow}c^{\dagger}_{k,1;\downarrow}|0\rangle,$$
$$|0,\uparrow\downarrow\rangle = c^{\dagger}_{k,2;\uparrow}c^{\dagger}_{k,2;\downarrow}|0\rangle,$$

where the states are indicated as in Ref. 15. This yields

$$\mathcal{H}_k = h_{11} \oplus (-h_{11}) \oplus \begin{pmatrix} h_{33} & 0 & t & t \\ 0 & -h_{33} & t & t \\ t & t & U & 0 \\ t & t & 0 & U \end{pmatrix} - \frac{1}{2}h_i(\mu_k + \mu_{k+1})\mathbf{1},$$

where

$$h_{11} = \frac{1}{2}(I_1 + I_2)(\mu_k + \mu_{k+1}) - h_e,$$
$$h_{33} = \frac{1}{2}(I_1 - I_2)(\mu_k - \mu_{k+1}),$$

and $\mathbf{1}$ is the unit matrix. The eigenvalues of the matrix $\mathcal{H}_k$ are given by

$$\mathcal{E}_1(\mu_k,\mu_{k+1}) = \frac{1}{2}(I_1 + I_2)(\mu_k + \mu_{k+1}) - h_e - \frac{h_i}{2}(\mu_k + \mu_{k+1}),$$
$$\mathcal{E}_2(\mu_k,\mu_{k+1}) = -\frac{1}{2}(I_1 + I_2)(\mu_k + \mu_{k+1}) - h_e - \frac{h_i}{2}(\mu_k + \mu_{k+1}),$$
$$\mathcal{E}_3(\mu_k,\mu_{k+1}) = \Lambda_1|\mu_k - \mu_{k+1}| - \frac{h_i}{2}(\mu_k + \mu_{k+1}),$$
$$\mathcal{E}_4(\mu_k,\mu_{k+1}) = \frac{1}{2}\left(U - \sqrt{U^2 + 16t^2}\right)|\mu_k + \mu_{k+1}| + \Lambda_2|\mu_k - \mu_{k+1}| - \frac{h_i}{2}(\mu_k + \mu_{k+1}),$$
$$\mathcal{E}_5(\mu_k,\mu_{k+1}) = \frac{1}{2}\left(U + \sqrt{U^2 + 16t^2}\right)|\mu_k + \mu_{k+1}| + \Lambda_3|\mu_k - \mu_{k+1}| - \frac{h_i}{2}(\mu_k + \mu_{k+1}),$$
$$\mathcal{E}_6(\mu_k,\mu_{k+1}) = U - \frac{h_i}{2}(\mu_k + \mu_{k+1}), \quad (3)$$

where Λ_i are the eigenvalues of the matrix,

$$\mathcal{L} = \begin{pmatrix} 0 & \frac{I_1 - I_2}{2} & 0 \\ \frac{I_1 - I_2}{2} & 0 & 2t \\ 0 & 2t & U \end{pmatrix}.$$

Finally, we obtain

$$\mathcal{Z}_k(\mu_k,\mu_{k+1}) = \sum_{i=1}^{6} \exp[-\beta\mathcal{E}_i(\mu_k,\mu_{k+1})].$$

We now carry out a decoration-iteration transformation for $\mathcal{Z}_k(\mu_k,\mu_{k+1})$:[1,2,15]

$$\mathcal{Z}_k(\mu_k,\mu_{k+1}) = A\exp[\beta R\mu_k\mu_{k+1} + \beta h_0(\mu_k+\mu_{k+1})/2]$$

where the parameters A, R, and h_0 are defined by

$$A = \left[\mathcal{Z}_k\left(\frac{1}{2},\frac{1}{2}\right)\mathcal{Z}_k\left(-\frac{1}{2},-\frac{1}{2}\right)\mathcal{Z}_k^2\left(\frac{1}{2},-\frac{1}{2}\right)\right]^{\frac{1}{4}},$$
$$\beta R = \ln\left[\mathcal{Z}_k\left(\frac{1}{2},\frac{1}{2}\right)\mathcal{Z}_k\left(-\frac{1}{2},-\frac{1}{2}\right)\mathcal{Z}_k^{-2}\left(\frac{1}{2},-\frac{1}{2}\right)\right],$$
$$\beta h_0 = \ln\left[\mathcal{Z}_k\left(\frac{1}{2},\frac{1}{2}\right)\mathcal{Z}_k^{-1}\left(-\frac{1}{2},-\frac{1}{2}\right)\right].$$

With this transformation, calculating the partition function of the Ising-Hubbard chain (2) reduces to calculating the partition function of an Ising chain with an interaction R and magnetic field h_0. Using the standard result for the partition function of an Ising chain,[18] we obtain the partition function (2) in the form

$$\mathcal{Z} = A^N(\lambda_1^N + \lambda_2^N),$$

where

$$\lambda_{1,2} = \exp\left(\frac{\beta R}{4}\right)\mathrm{ch}\left(\frac{\beta h_0}{2}\right) \pm\sqrt{\exp\left(\frac{\beta R}{2}\right)\mathrm{sh}^2\left(\frac{\beta h_0}{2}\right)+\exp\left(-\frac{\beta R}{2}\right)}.$$

In the thermodynamic limit, the free energy per primitive cell is given by

$$f = -\frac{1}{\beta}\ln A - \frac{1}{\beta}\ln\lambda_1.$$

From the free energy we calculate the energy s and the specific heat c:

$$s = k_B\beta^2\left(\frac{\partial f}{\partial\beta}\right)_{h_i,h_e}, \quad c = -\beta\left(\frac{\partial s}{\partial\beta}\right)_{h_i,h_e}.$$

Calculating the magnetization $m_i = \frac{1}{2}\langle\mu_k+\mu_{k+1}\rangle$ and correlation function $q_{ii}(n) = \langle\mu_k\mu_{k+n}\rangle$ of the Ising spins of an Ising-Hubbard chain reduces to calculating these same characteristics for an Ising chain with an interaction R and magnetic field h_0. Thus, for m_i and $q_{ii}(n)$, we use the standard results.[18] The magnetization of the electronic subsystem $m_e = \frac{1}{2}\langle S_{k,1}+S_{k,2}\rangle$ is obtained by differentiating the partition function $\mathcal{Z}$ with respect to h_e.[19] Thus, calculating the magnetization m_e reduces to differentiating the parameters of the decoration-iteration transformation with respect to h_e:

$$m_e = \frac{1}{2\beta}\left(\frac{1}{A}\frac{\partial A}{\partial h_e} + q_{ii}(1)\frac{\partial(\beta R)}{\partial h_e} + m_i\frac{\partial(\beta h_0)}{\partial h_e}\right).$$

Given the magnetizations of the subsystems, we now determine the total magnetization,

$$m = (m_i + 2m_e)/3.$$

Note that in the magnetization (m) processes, m_i and m_e will have the same saturation value $m_S = 1/2$. The magnetic susceptibility in a magnetic field h has the following structure:

$$\chi = \frac{dm}{dh} = \frac{1}{3}\left(\frac{\partial m_i}{\partial h_i}\frac{dh_i}{dh} + \frac{\partial m_i}{\partial h_e}\frac{dh_e}{dh}\right) + \frac{2}{3}\left(\frac{\partial m_e}{\partial h_i}\frac{dh_i}{dh} + \frac{\partial m_e}{\partial h_e}\frac{dh_e}{dh}\right).$$

With this we conclude our examination of the basic points concerning an exact calculation of the thermodynamic characteristics of an Ising-Hubbard chain.

III. RESULTS AND DISCUSSION

In the above analytic expressions, the Ising interaction can be ferromagnetic or antiferromagnetic. Let us examine the properties of a chain for the case of an antiferromagnetic Ising interaction ($I_1, I_2 \geq 0$) when the system is geometrically frustrated. With loss of generality, we take $I_1 \geq I_2$ and introduce the difference between the Ising interactions, $\Delta I = I_1 - I_2$, as in Ref. 15. We consider a magnetic field that is the same for the Ising and electronic spins, i.e., $h = h_i = h_e$. In order to reduce the number of free parameters in the model, we proceed (as in Ref. 15) to the dimensionless parameters

$$\tilde{t} = \frac{t}{I_1}, \quad \tilde{U} = \frac{U}{I_1}, \quad \tilde{h} = \frac{h}{I_1}, \quad \Delta\tilde{I} = \frac{\Delta I}{I_1},$$

where $I_1 \neq 0$. The parameter $\Delta\tilde{I}$ has a physical significance in the region $0 \leq \Delta\tilde{I} \leq 1$ and characterizes the possible degree of asymmetry of the Ising interactions for the assumed distortion of the diamond.

We first consider the properties of the ground state of the system. The ground state corresponds to a minimum energy of a primitive cell (3) for all the possible values of μ_k and μ_{k+1}. The energies (3) in dimensionless form $\tilde{\mathcal{E}}_i(\mu_k,\mu_{k+1}) = \mathcal{E}_i(\mu_k,\mu_{k+1})/I_1$ are functions of the four model parameters: $\tilde{t}, \tilde{U}, \Delta\tilde{I}, \tilde{h}$. Depending on these parameters, the ground state can be one of four states, such as those without Coulomb repulsion,[15] specifically: a saturated paramagnetic state (SPA), a ferrimagnetic state (FRI), an unsaturated paramagnetic state (UPA), and a node antiferromagnetic state (NAF). The dimensionless energies of the states per primitive cell are

$$\tilde{\mathcal{E}}_{\mathrm{SPA}} = \frac{1}{2}(2 - \Delta\tilde{I} - 3\tilde{h}),$$
$$\tilde{\mathcal{E}}_{\mathrm{FRI}} = \frac{1}{2}(-2 + \Delta\tilde{I} - \tilde{h}),$$
$$\tilde{\mathcal{E}}_{\mathrm{UPA}} = \frac{1}{2}(\tilde{U} - \sqrt{\tilde{U}^2 + 16\tilde{t}^2} - \tilde{h}),$$
$$\tilde{\mathcal{E}}_{\mathrm{NAF}} = \min\{\tilde{\Lambda}_i, i = 1,2,3\},$$

where $\tilde{\Lambda}_i$ are the eigenvalues of the matrix $\tilde{\mathcal{L}} = \mathcal{L}/I_1$. These states correspond to the following wave functions:

$$|\mathrm{SPA}\rangle = \prod_{k=1}^{N}|+\rangle_k|\uparrow,\uparrow\rangle_{k,1;k,2},$$
$$|\mathrm{FRI}\rangle = \prod_{k=1}^{N}|-\rangle_k|\uparrow,\uparrow\rangle_{k,1;k,2},$$
$$|\mathrm{UPA}\rangle = \prod_{k=1}^{N}|+\rangle_k[\Psi_{\mathrm{UPA}}]_{k,1;k,2},$$
$$|\mathrm{NAF}\rangle = \prod_{k=1}^{N}|(-)^{n=\{^k_{k+1}}>_k\left[\Psi_{\mathrm{NAF}}^{(-)^n}\right]_{k,1;k,2},$$

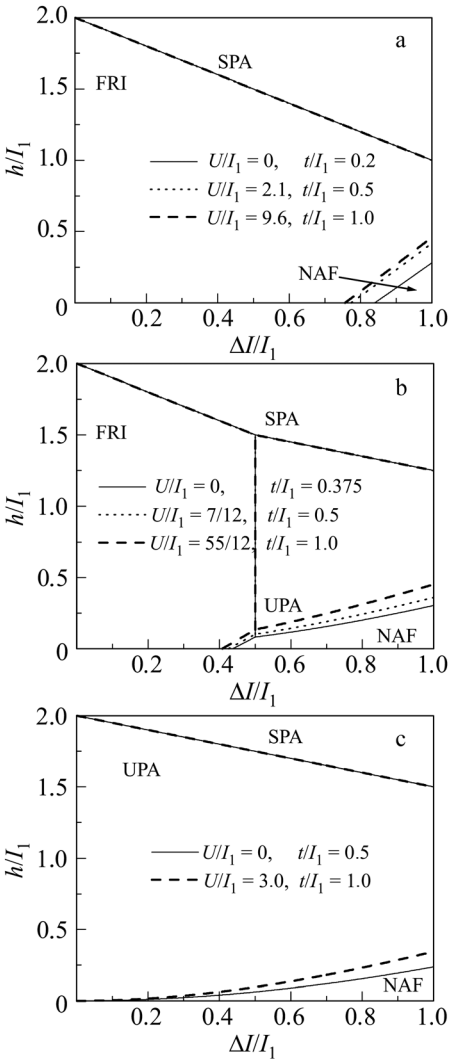

FIG. 2. Phase diagram of the $(\Delta\tilde{I}, \tilde{h})$ ground state. There are three possible typical diagrams. Each diagram shows the curves along which states coexist for several sets of values of $\tilde{U}$ and $\tilde{t}$. The results for $\tilde{U} = 0$ are the same as in Ref. 15.

where the functions $|\pm\rangle_k$ describe the states of the Ising spins μ_k: $|+\rangle = |\uparrow\rangle$ and $|-\rangle = |\downarrow\rangle$. To write down the wave functions for the doubly degenerate state NAF, we use the expression $(-)^{n=\{^k_{k+1}}$, where $(-)^n$ denotes the sign of the number $(-1)^n$. The remaining notation is

$$\Psi_{\mathrm{UPA}} = A_{\mathrm{UPA}}(|\uparrow,\downarrow\rangle + |\downarrow,\uparrow\rangle) + B_{\mathrm{UPA}}(|\uparrow\downarrow,0\rangle + |0,\uparrow\downarrow\rangle),$$

$$\Psi^{+}_{\mathrm{NAF}} = A^{+}_{\mathrm{NAF}}|\uparrow,\downarrow\rangle + A^{-}_{\mathrm{NAF}}|\downarrow,\uparrow\rangle + B_{\mathrm{NAF}}(|\uparrow\downarrow,0\rangle + |0,\uparrow\downarrow\rangle),$$

where

$$A_{\mathrm{UPA}} = \frac{1}{2}\sqrt{1 + \frac{\tilde{U}}{\sqrt{\tilde{U}^2 + 16\tilde{t}^2}}},$$

$$B_{\mathrm{UPA}} = -\frac{1}{2}\sqrt{1 - \frac{\tilde{U}}{\sqrt{\tilde{U}^2 + 16\tilde{t}^2}}},$$

$$A^{\pm}_{\mathrm{NAF}} = \frac{(\tilde{\mathcal{E}}_{\mathrm{NAF}} \pm \frac{1}{2}\Delta\tilde{I})(\tilde{\mathcal{E}}_{\mathrm{NAF}} - \tilde{U})}{\sqrt{2\Phi_{\mathrm{NAF}}}}, \quad B_{\mathrm{NAF}} = \frac{2\tilde{t}\tilde{\mathcal{E}}_{\mathrm{NAF}}}{\sqrt{2\Phi_{\mathrm{NAF}}}},$$

$$\Phi_{\mathrm{NAF}} = \left(\tilde{\mathcal{E}}^2_{\mathrm{NAF}} + \frac{1}{4}\Delta\tilde{I}^2\right)(\tilde{\mathcal{E}}_{\mathrm{NAF}} - \tilde{U})^2 + 4\tilde{t}^2\tilde{\mathcal{E}}^2_{\mathrm{NAF}}.$$

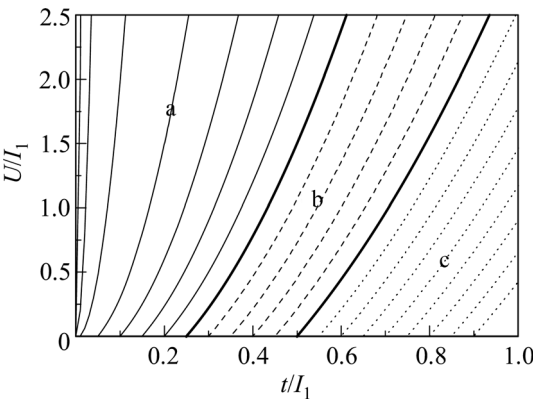

FIG. 3. A diagram indicating the influence of jumps and repulsion $(\tilde{t}, \tilde{U})$ in the form of a phase diagram for the $(\Delta\tilde{I}, \tilde{h})$ ground state; (a), (b), and (c) denote the regions in which the types of $(\Delta\tilde{I}, \tilde{h})$ phase diagrams shown in Fig. 2 exist. The regions are covered by "equi-diagram" contours: thin smooth (a), dashed (b), and dotted (c). The boundaries between the regions are indicated by thick, smooth "equi-diagram" curves.

We now consider the phase diagram of the ground state in the $(\Delta\tilde{I}, \tilde{h})$ plane. Its form is determined by the parameters $\tilde{t}$ and $\tilde{U}$. Depending on these parameters, three typical phase diagrams similar to those without repulsion can be realized (Fig. 2).[15] The first such phase diagram (Fig. 2(a)) exists for

$$\tilde{t} \le \frac{1}{4}\sqrt{1 + 2\tilde{U}}.$$

In zero field the FRI and NAF states coexist when $\Delta\tilde{I} = \Delta\tilde{I}_{\mathrm{F.N}}$, which is given by

$$\Delta\tilde{I}_{\mathrm{F.N}} - 2 - 2\tilde{\mathcal{E}}_{\mathrm{NAF}} = 0.$$

The second typical phase diagram (Fig. 2(b)) exists for

$$\frac{1}{4}\sqrt{1 + 2\tilde{U}} < \tilde{t} < \frac{1}{2}\sqrt{1 + \tilde{U}}.$$

The FRI and UPA states coexist on the line $\Delta\tilde{I} = \Delta\tilde{I}_{\mathrm{F|U}}$, where

$$\Delta\tilde{I}_{\mathrm{F|U}} = \tilde{U} - \sqrt{\tilde{U}^2 + 16\tilde{t}^2} + 2.$$

The third typical phase diagram (Fig. 2(c)) exists for

$$\frac{1}{2}\sqrt{1 + \tilde{U}} \le \tilde{t}.$$

If we set $\tilde{U} = 0$ in the above expressions characterizing the phase diagram, then they coincide with the corresponding expressions in Ref. 15.

A qualitative discussion of the phase diagrams for the ground state in Fig. 2 can be found in Ref. 15. Here we supplement that with a discussion of some interesting properties of the ground state that show up under certain conditions. We begin with the line on which the FRI and SPA states coexist. The node antiferromagnetic state NAF_+ also exists on this line, with an energy $\tilde{\mathcal{E}}_{\mathrm{NAF}_+} = -\tilde{h}$ and wave function

$$|\mathrm{NAF}_+\rangle = \prod_{k=1}^{N} |(-)^{n=\{^k_{k+1}\rangle_{k|\uparrow,\uparrow\rangle k,1;k,2}}$$

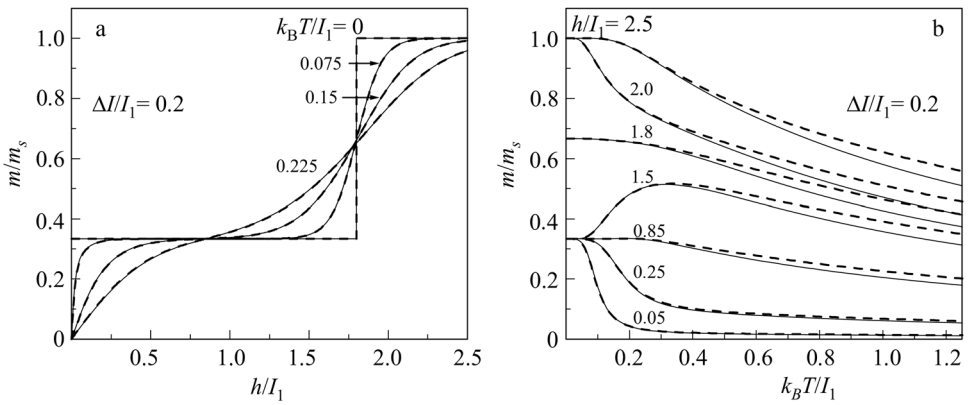

FIG. 4. The total magnetization as a function of (a) magnetic field for different temperatures and (b) temperature for different magnetic fields (b) in the case where the FRI state is the zero field ground state. The smooth curves show the results for $\tilde{U} = 0$ and $\tilde{t} = 0.375$, which coincide with the corresponding results from Ref. 15. The dashed curves are the results for $\tilde{U} = 55/12$ and $\tilde{t} = 1.0$.

The behavior of the Ising subsystem is described by these characteristics:

$$\beta R = \beta h_0 = 0, \quad m_i = 0, \quad q_{ii}(n) = 0. \tag{4}$$

This indicates that the Ising spins are effectively free, i.e., they can be in one of two states with equal probability: $|\uparrow\rangle$ and $|\downarrow\rangle$. Here the interstitial electron pairs are in a $|\uparrow,\uparrow\rangle$ state. Geometrically frustrated Ising-Heisenberg states are known to have a monomer-dimer type ground state, in which the Ising spins are effectively free, while the pairs of interstitial Heisenberg spins are in a certain intricate state, known as frustrated states (FRU).[8–10] Using this terminology, we refer to this ground state as a frustrated ferromagnetic state, FRU_+:

$$|\mathrm{FRU}_+\rangle = \prod_{k=1}^{N} |\pm\rangle_k |\uparrow,\uparrow\rangle_{k,1;k,2}.$$

The FRU_+ state differs from the frustrated states if Ising-Heisenberg states described in Refs. 8–10 in that all of the spins in its primitive cell are semiclassically ordered. This occurs because of the influence of the strong magnetic field. The effective freedom of the Ising spin determines the macroscopic degeneracy of the FRU_+ state, which gives a residual entropy $s_{\mathrm{res}} = k_B \ln 2$.

At the point $(\Delta\tilde{I}_{\mathrm{F|U}}, 2 - \Delta\tilde{I}_{\mathrm{F|U}})$, i.e., the end of the line on which the FRI and SPA states coexists (Fig. 2(b)), the state of the system differs from FRU_+. At this point the state of the Ising subsystem is described by the following parameters:

$$\beta R = \beta h_0 = \ln 2, \quad m_i = \frac{m_s}{\sqrt{5}}, \quad q_{ii}(n) = \frac{1}{20} + \frac{1}{5}\left(\frac{3-\sqrt{5}}{3+\sqrt{5}}\right)^n.$$

Thus, the Ising spins are no longer free. This state of the Ising spins with $R = h_0 = 0$ shows up in the form of a linear component in the temperature dependences of the parameters R and $\mathrm{h_0}$ which affects the formation of the Ising spin state in the limit $T \to 0$. This ground state has a residual entropy $s_{\mathrm{res}} = k_g \ln[(3+\sqrt{5})/2]$ that is greater than for the FRU_+ state.

We now consider the properties of the ground state at the point $(\Delta\tilde{I}_{F.N}, 0)$. In this state the Ising spins behave freely, in accordance with Eqs. (4), while the state of the interstitial electron pairs is determined by the states of the neighboring Ising spins and can, with equal probabilities, be one of four states: $|\uparrow,\uparrow\rangle$, $|\downarrow,\downarrow\rangle$, Ψ^{-}_{NAF}, and Ψ^{+}_{NAF}. This ground state is macroscopically degenerate: $s_{\mathrm{res}} = k_g \ln 2$. In many regards, this state is similar to the frustrated states from Refs. 8–10 and the FRU_+ state. However, unlike these states, it is not a monomer-dimer type state. The ground state has essentially the same properties as those at the point $(\Delta\tilde{I}_{\mathrm{F.N}}, 0)$, at the point where the FRI, UPA, and NAF states coexist $(\Delta\tilde{I}_{\mathrm{F|U}}, \tilde{h}_{\mathrm{F|N|U}})$, where $\tilde{h}_{\mathrm{F|N|U}} = \Delta\tilde{I}_{\mathrm{F|U}} - 2 - 2\mathcal{E}_{\mathrm{NAF}}$.

The free behavior of the Ising spins at the points $(\Delta\tilde{I}_{\mathrm{F.N}}, 0)$ and $(\Delta\tilde{I}_{\mathrm{F|U}}, \tilde{h}_{\mathrm{F|N|U}})$ vanishes when they coincide, which can only happen at the point (0,0) when $\tilde{t} = \sqrt{1+\tilde{U}}/2$ (Fig. 2(c)). In this case, the Ising subsystem has the following properties:

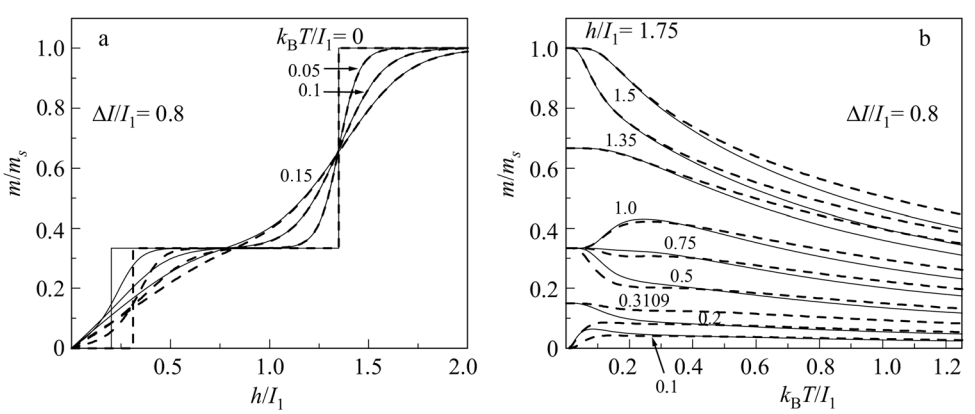

FIG. 5. The total magnetization as a function of (a) magnetic field for different temperatures and (b) temperature for different magnetic fields (b) in the case where the NAF state is the zero field ground state. The smooth curves show the results for $\tilde{U} = 0$ and $\tilde{t} = 0.375$, which coincide with the corresponding results from Ref. 15. The dashed curves are the results for $\tilde{U} = 55/12$ and $\tilde{t} = 1.0$.

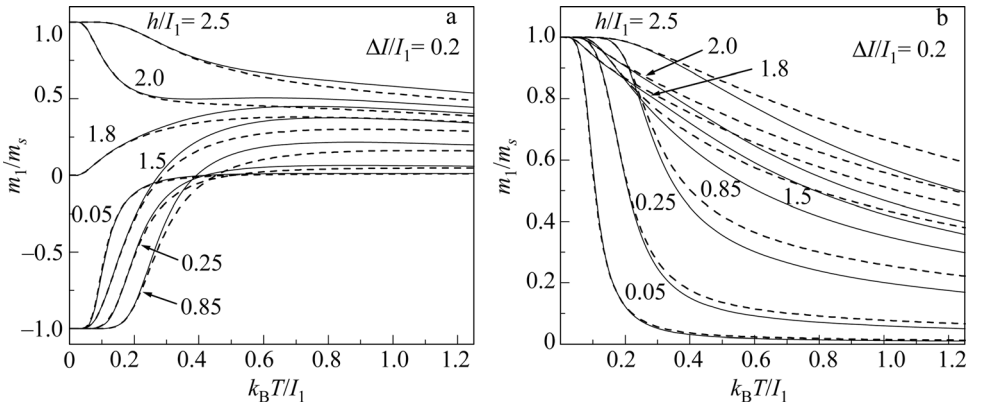

FIG. 6. The magnetizations of the Ising (a) and electronic (b) subsystems as functions of temperature for different magnetic fields. These magnetizations form the total magnetization in Fig. 4(b). The smooth curves show the results for $\tilde{U}=0$ and $\tilde{t}=0.375$. The dashed curves show the results for $\tilde{U}=55/12$ and $\tilde{t}=1.0$.

$$\beta R = 2\ln 2, \quad \beta h_0 = 0, \quad m_i = 0, \quad q_{ii}(n) = \frac{1}{4}\frac{1}{3^n}.$$

The existence of a ferromagnetic correlation between the Ising spins in this state because of the linear component in the temperature dependence of the parameter R. This state has a residual entropy of $s_{\text{res}} = k_g \ln 3$.

When $\tilde{t} > \sqrt{1+\tilde{U}}/2$, the state FRU is frustrated at the point (0,0), where

$$|\text{FRU}\rangle = \prod_{k=1}^{N} |\pm\rangle_k [\Psi_{\text{UPA}}]_{k,1;k,2}.$$

In this state a pair of interstitial electrons lies in a complicated state similarly to a pair of Heisenberg spins in frustrated Ising-Heisenberg states.[8–10] The residual entropy equals $k_B \ln 2$.

Now we examine the effect of the Coulomb repulsion $\tilde{U}$ on the phase diagram $(\Delta\tilde{I}, \tilde{h})$. The repulsion $\tilde{U}$ affects it, as do the jumps $\tilde{t}$, through a change in the energies $\mathcal{E}_{\text{UPA}}$ and $\mathcal{E}_{\text{NAF}}$. If a change in $\tilde{U}$ is accompanied by a change in $\tilde{t}$ while maintaining a fixed energy $\mathcal{E}_{\text{UPA}}$, then the readjustment of the phase diagram $(\Delta\tilde{I}, \tilde{h})$ will be much simpler. In particular, the line on which the FRI and UPA ground states coexists does not change its position $\Delta\tilde{I}_{\text{F|N}}$. Assigning an energy $\tilde{\mathcal{E}}_{\text{UPA}}$ in this regime to the point $(\tilde{t}=\tilde{t}^*, \tilde{U}=0)$, where $\tilde{t}^*$ is the jump integral in the theory without repulsion, we obtain the condition for the variation in $\tilde{U}$:

$$\sqrt{\tilde{U}^2 + 16\tilde{t}^2} - \tilde{U} = 4\tilde{t}^*. \tag{5}$$

The effect of $\tilde{U}$ in the regime (5) on the phase diagram $(\Delta\tilde{I}, \tilde{h})$ is shown in Fig. 2, where in each of the three cases (a, b, and c) the sets of parameters $\tilde{U}$ and $\tilde{t}$ satisfy condition (5) with a certain $\tilde{t}^*$. Under this influence, the typical form of the phase diagram specified by the parameter $\tilde{t}^*$ does not change, and the lines on which the NAF state coexists with the FRI and UPA states only shift slightly. In this sense, the diagrams for all pairs of $\tilde{U}$ and $\tilde{t}$, which corresponding to a single $\tilde{t}$ according to Eq. (5), are equivalent to one another. Using this fact, we construct a $(\tilde{t}, \tilde{U})$ diagram that reflects the effect of repulsion and jumps on the $(\Delta\tilde{I}, \tilde{h})$ phase diagram. The $(\tilde{t}, \tilde{U})$ diagram is shown in Fig. 3. It is covered with "equi-diagram" contours (5). In this diagram it is easy to see that increasing $\tilde{U}$ for fixed $\tilde{t}$ changes the phase diagram similarly to a reduction in $\tilde{t}$ for fixed $\tilde{U}$. This means that the effect of repulsion on the ground state essentially involves a weakening of the effect of the jump intensity.

We now examine the influence of repulsion on the field and temperature dependences of the thermodynamic characteristics. For this purpose, we consider the change in the thermodynamic characteristics with changing repulsion in the regime (5) in comparison to the results of Ref. 15. We consider the sets of values of $\tilde{U}$ and $\tilde{t}$ for which the ground state phase diagram is shown in Fig. 2(b). We begin with the magnetization process at low temperatures. The influence of repulsion depends on which state, FRI or NAF, is the ground state in zero field. In the case of an FRI ground state, the effect of repulsion can hardly be seen (Fig. 4(a)), while for an NAF ground state it shows up strongly (Fig. 5(a)). This is because the increased repulsion leads to a rise in the critical field at which the zero magnetization plateau transforms to a plateau at 1/3 the saturation magnetization (Fig. 5(a)). As a result, the magnetization curve at a temperature of 0.05 for $\tilde{U}=55/12$, as opposed to $\tilde{U}=0$,[15] manifests spreading of the zero magnetization plateau (Fig. 5(a)). The increased field interval with zero magnetization is also reflected in the behavior of the low-temperature magnetization curves at the corresponding magnetic fields (Fig. 5(b)).

Regardless of which ground state occurs in zero field, an increase in the repulsion shifts the high-temperature total magnetization upward (Figs. 4(b) and 5(b)). In order to understand the mechanism for this shift, we examine the

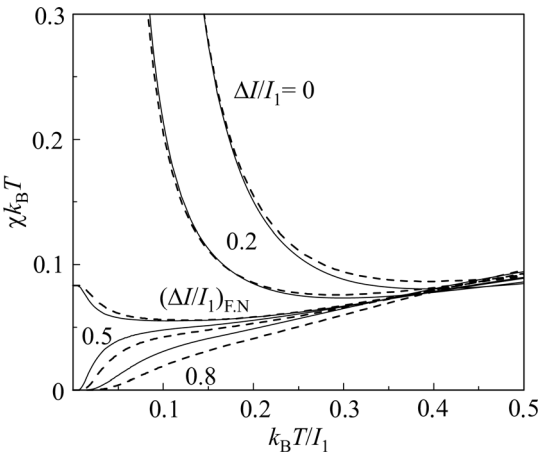

FIG. 7. Zero field magnetic susceptibility times the temperature as a function of temperature. The smooth curves show the results for $\tilde{U}=0$ and $\tilde{t}=0.375$, which coincide with the corresponding results from Ref. 15. The dashed curves show the results for $\tilde{U}=55/12$ and $\tilde{t}=1.0$.

temperature dependences of the magnetizations of the Ising and electronic subsystems (Fig. 6). It turns out that, with increasing repulsion, the high-temperature magnetization curves for these subsystems shift in opposite directions: the curve for the Ising subsystem shifts downward (Fig. 6(a)) and that for the electronic subsystem shifts upward (Fig. 6(b)). Since the electronic subsystem is twice the size of the Ising subsystem, it determines the direction of the shift in the total magnetization. An analysis of the numerical results showed that this decrease in the high-temperature magnetization of the Ising spins is related to a drop in the effective magnetic field h_0. The increase in the high-temperature magnetization of the electronic subsystem, on the other hand, can be explained by an increase in at least two of the high energies in the spectrum of the hamiltonian $\mathcal{H}_k$ (3), which correspond to zero magnetization of an interstitial electron pair, specifically, $\mathcal{E}_5$ and $\mathcal{E}_6$.

If the asymmetry $\Delta\tilde{I}$ of the Ising interactions lies within a certain neighborhood of the critical point $\Delta\tilde{I}_{\mathrm{F.N}}$ or in the region of an NAF ground state, then the low-temperature magnetic susceptibility curves multiplied by the temperature ($\chi k_B T$) undergo significant changes in zero field under the influence of repulsion (Fig. 7). These changes may be related to a drop in the energy of the NAF ground state with increasing repulsion, similar to the change in the magnetization curves. The high-temperature $\chi k_B T$ curves shift to higher values with increasing repulsion.

We now consider the effect of repulsion on the temperature dependence of the specific heat in zero field. Two peaks have been found in this dependence when $\tilde{U} = 0$:[15] a main peak and a secondary peak nearer to zero temperature (Fig. 8), whose appearance has been attributed to thermal excitation is responsible for transitions between the FRI and NAF states. When $\tilde{U} = 55/12$, as opposed to $\tilde{U} = 0$, the high-temperature dependence of the specific heat in Fig. 8 has a principal maximum of perceptibly lower height and, additionally, a very broad, low maximum at a considerably higher temperature than that of the main peak. This additional peak appears only with strong repulsion. When $\tilde{U} = 7/12$ it has not yet shown up, and the main peak is just readjusted, as it decreases, broadens, and shifts slightly to higher temperatures. All of this indicates that the principal maximum is related not only to the thermal excitations which destroy the dimer-like antiferromagnetic correlations between the Ising and electronic spins caused by the strongest Ising interaction I_1,[15] but also to the thermal excitations which destroy the antiferromagnetic correlations between the spins of an interstitial electron pair and overcome the single-position Coulomb repulsion of the electrons. With changing repulsion, the low-temperature part of the specific heat, which includes the secondary maximum, is essentially unchanged when $\Delta\tilde{I}$ lies in the region of the FRI ground state (Fig. 8(a)), but changes significantly when $\Delta\tilde{I}$ lies within the region of the NAF ground state (Fig. 8(b)).

Besides having a structure with a single secondary peak (Fig. 8), the low-temperature specific heat in zero field can have a structure with two secondary peaks (Fig. 9). The additional peak in the specific heat nearest to zero temperature (Fig. 9) is not related to repulsion, as it also exists for $\tilde{U} = 0$. This

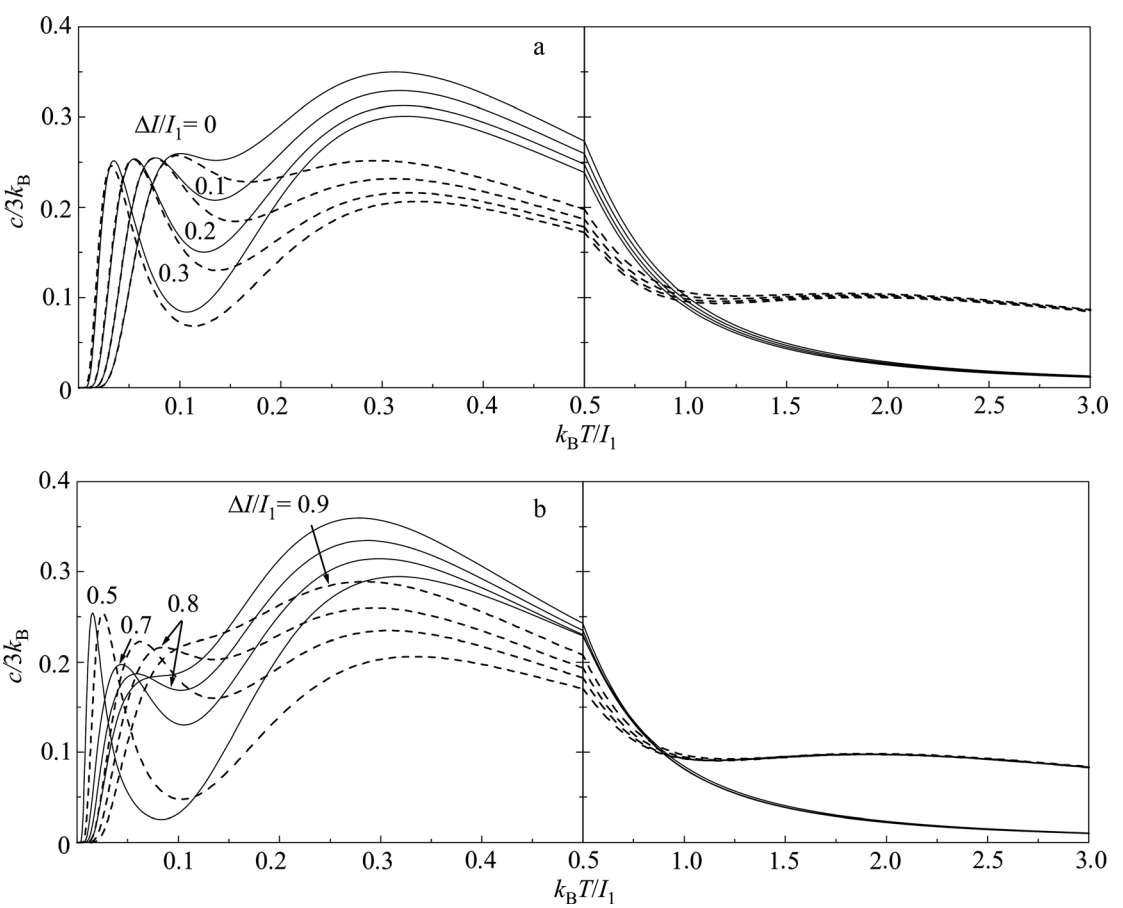

FIG. 8. Zero field specific heat as a function of temperature for two cases: FRI as ground state (a) and NAF as ground state (b). The smooth curves show the results for $\tilde{U} = 0$ and $\tilde{t} = 0.375$, which coincide with the corresponding results from Ref. 15. The dashed curves show the results for $\tilde{U} = 55/12$ and $\tilde{t} = 1.0$.

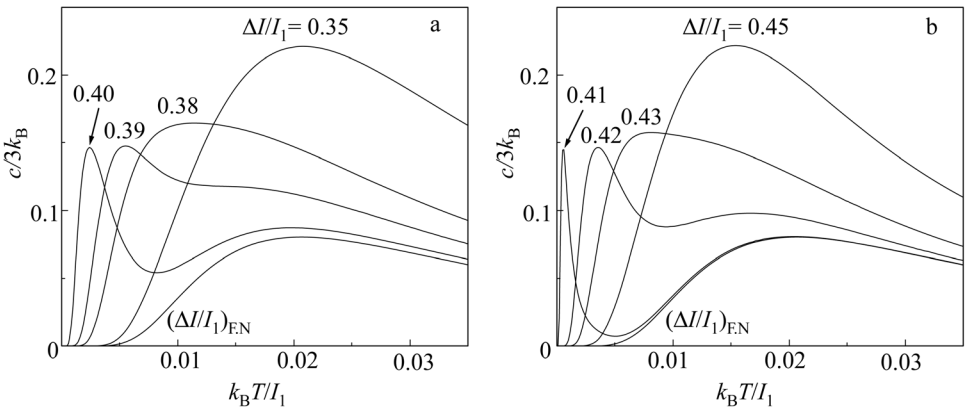

FIG. 9. Zero field specific heat as a function of temperature for $\tilde{t} = 1.2$ and $\tilde{U} = 55/12$ with different $\Delta\tilde{I}$ within a small neighborhood of the critical point $\Delta\tilde{I}_{F.N}$. Shown here is the approach of $\Delta\tilde{I}$ from the region of an FRI ground state to the critical point $\Delta\tilde{I}_{F.N}$ (a) and the separation of $\Delta\tilde{I}$ from the critical point $\Delta\tilde{I}_{F.N}$ into the depth of an NAF ground state (b).

maximum shows up when the parameter $\Delta\tilde{I}$ lies within a fairly small neighborhood of the critical point $\Delta\tilde{I}_{F.N}$. If this region is crossed from the FRI ground state, then the secondary maximum in the specific heat splits into two peaks. On closer approach to the critical point $\Delta\tilde{I}_{F.N}$, the maximum corresponding to the lower temperature rapidly approaches zero temperature and vanishes at the critical point (Fig. 9(a)). Beyond the critical point in the NAF state it again shows up near zero temperature. With increasing distance from the critical point it rapidly approaches the other low-temperature peak and merges with it (Fig. 9(b)). This implies that the maximum which vanishes at the critical point $\Delta\tilde{I}_{F.N}$ is related precisely to thermal excitations which are responsible for transitions between the FRI and NAF states. On the other hand, the low-temperature peak which does not vanish at the critical point $\Delta\tilde{I}_{F.N}$ is related to excitations which are responsible for transitions between the FRI and UPA states and the NAF and UPA states.

IV. CONCLUSION

The thermodynamic characteristics of distorted diamond Ising-Hubbard chains (free energy, entropy, specific heat, magnetization of the Ising and electronic subsystems, and magnetic susceptibility), including on-site Coulomb repulsion, have been calculated using a decoration-iteration transformation method. The effect of Coulomb repulsion on the ground state has been studied for the case of an antiferromagnetic Ising interaction where the system is geometrically frustrated and, in the regime of Eq. (5), on the thermodynamics: the field and temperature dependences of the magnetization, and the magnetic susceptibility and specific heat as functions of temperature.

The same four ground states (SPA, FRI, UPA, NAF) and the same three typical phase diagrams for the ground state $(\Delta\tilde{I}, \tilde{h})$ as systems without Coulomb repulsion[15] are realized in systems with Coulomb repulsion. A change in the repulsion, which is accompanied by changes in the jump intensity such that the energy of the UPA state is unchanged, does not change the type of the ground state phase diagram, but only shifts the boundary curves for the NAF ground state region. The effect of repulsion and jumps on the form of the $(\Delta\tilde{I}, \tilde{h})$ phase diagram shows up in the $(\tilde{t}, \tilde{U})$ diagram. Thus, we have obtained a complete description of the properties of the ground state as functions of the model parameters. We have found that increasing Coulomb repulsion effectively weakens the influence of the rate of jumps into the ground state.

We have studied the properties of the ground state along several critical curves and at critical points in the $(\Delta\tilde{I}, \tilde{h})$ phase diagrams. On the curve where the FRI and SPA states coexist and for $\tilde{t} > \sqrt{1+\tilde{U}}/2$ at the point (0,0), a frustrated state is realized. At the point $(\Delta\tilde{I}_{F|U}, 2 - \Delta\tilde{I}_{F|U})$, where the curve on which the FRI and SPA states coexist comes to an end, the ground state differs from the frustrated stage owing to the presence of a linear component in the temperature dependences of R and h_0 that determines the ground state of the Ising subsystem when $R = h_0 = 0$. This state has a residual entropy $s_{res} = k_B \ln[(3+\sqrt{5})/2]$ that is greater than that of the frustrated state. At the points $(\Delta\tilde{I}_{F.N}, 0)$ and $(\Delta\tilde{I}_{F|U|}, \tilde{h}_{F|N|U})$ the Ising states are effectively free, while the interstitial state of an electron pair is uniquely determined by the states of the neighboring Ising spins. When these points coincide at the point (0,0), the Ising spins are no longer effectively free. In addition, this ground state has the highest residual entropy, $s_{res} = k_B \ln 3$.

The influence of Coulomb repulsion on the low-temperature magnetization process and on the low-temperature magnetization and magnetic susceptibility curves is perceptible near the boundary of the NAF ground state because it is shifted. The high-temperature magnetization curves of the subsystems shift in opposite ways with increasing Coulomb repulsion: the electronic subsystem toward higher magnetization and the Ising subsystem, toward lower magnetization. Here the high-temperature curve for the total magnetization shifts toward higher values. The high-temperature magnetic susceptibility curve is shifted similarly. Increasing Coulomb repulsion lowers the height of the principal maximum in the specific heat, and when the Ising interactions from the region of the NAF ground state are asymmetric, a secondary peak in the specific heat reposition itself. The strong repulsion controls the additional peak in the specific heat, which lies considerably above the temperature of the principal maximum.

It has been found that, regardless of the existence of Coulomb repulsion, when the asymmetries of the Ising interactions fall within a sufficiently small neighborhood of the critical point $\Delta\tilde{I}_{F,N}$, the specific heat in zero field has two low-temperature peaks. The closest peak to zero temperature vanishes at the critical point $\Delta\tilde{I}_{F,N}$; that is, it is related to thermal excitations which are responsible for transitions between the FRI and NAF states.

The author thanks O. V. Derzhko and V. M. Verkholyak for a discussion and useful comments.

[a)]Email: lisnyj@icmp.lviv.ua

[1]I. Syozi, Prog. Theor. Phys. **6**, 341 (1951).
[2]M. Fisher, Phys. Rev. **113**, 969 (1959).
[3]T. Kaneyoshi, Prog. Theor. Phys. **97**, 407 (1997).
[4]V. R. Ohanyan and N. S. Ananikian, Phys. Lett. A **307**, 76 (2003).
[5]J. S. Valverde, O. Rojas, and S. M. de Souza, Physica A **387**, 1947 (2008).
[6]J. Strečka and M. Jaščur, J. Phys.: Condens. Matter **15**, 4519 (2003).
[7]J. Strečka, M. Jaščur, M. Hagiwara, K. Minami, Y. Narumi, and K. Kindo, Phys. Rev. B **72**, 024459 (2005).
[8]L. Čanová, J. Strečka, and M. Jaščur, J. Phys.: Condens. Matter **18**, 4967 (2006).
[9]L. Čanová, J. Strečka, and T. Lučivjanský, Condens. Matter Phys. **12**, 353 (2009).
[10]V. Ohanyan, Condens. Matter Phys. **12**, 343 (2009).
[11]J. S. Valverde, O. Rojas, and S. M. de Souza, J. Phys.: Condens. Matter **20**, 345208 (2008).
[12]D. Antonosyan, S. Bellucci, and V. Ohanyan, Phys. Rev. B **79**, 014432 (2009).
[13]H. Kikuchi, Y. Fujii, M. Chiba, S. Mitsudo, T. Idehara, T. Tonegawa, K. Okamoto, T. Sakai, T. Kuwai, and H. Ohta, Phys. Rev. Lett. **94**, 227201 (2005).
[14]H. Kikuchi, Y. Fujii, M. Chiba, S. Mitsudo, T. Idehara, T. Tonegawa, K. Okamoto, T. Sakai, T. Kuwai, and H. Ohta, Prog. Theor. Phys. Suppl. **159**, 1 (2005).
[15]M. S. S. Pereira, F. A. B. F. de Moura, and M. L. Lyra, Phys. Rev. B **77**, 024402 (2008).
[16]O. Derzhko, A. Honecker, and J. Richter, Phys. Rev. B **79**, 054403 (2009).
[17]M. S. S. Pereira, F. A. B. F. de Moura, and M. L. Lyra, Phys. Rev. B **79**, 054427 (2009).
[18]R. Baxter, *Exactly Solvable Models in Statistical Mechanics* [Russian translation] (Mir, Moscow, 1985).
[19]B. Lisnii, Ukr. J. Phys. **53**, 708 (2008).

Translated by D. H. McNeill